Electronic Structures of Bis(benzene)chromium and the C_{2h} and C_{2v} Isomers of Bis(naphthalene)chromium

Joseph H. Osborne,[1a] William C. Trogler,*[1a] Pascale D. Morand,[1b] and Colin G. Francis*[1b]

Department of Chemistry, D-006, University of California at San Diego, La Jolla, California 92093, and Department of Chemistry, University of Southern California, Los Angeles, California 90089

Received May 27, 1986

Molecular orbital calculations using the SCF-Xα-DV method have been performed for bis(benzene)-chromium and for bis(naphthalene)chromium in two possible geometries, C_{2h} and C_{2v}. The bonding in $Cr(\eta\text{-}C_6H_6)_2$ can be described in a ligand field context based on pseudooctahedral Cr d orbitals ($t_{2g} \rightleftharpoons 3e_{2g}$, $4a_{1g}$ and $e_g \rightleftharpoons 4e_{1g}$). The filled e_{1g} π orbitals of the benzene ligands donate electrons into the empty Cr $4e_{1g}$ d orbitals. The filled Cr $3e_{2g}$ orbitals delocalize into the empty benzene e_{2u} (π^*) orbitals of δ symmetry with respect to the metal. In both the C_{2v} and C_{2h} isomers of $Cr(\eta^6\text{-}C_{10}H_8)_2$ the HOMO is a metal d_{z^2} orbital ($16a_g$ or $16a_1$) that points toward the center of the η^6-bound ring similar to that found for $Cr(\eta\text{-}C_6H_6)_2$. Most metal–arene bonding occurs in lower lying orbitals. The calculated Cr charge of 0.744 (0.708) in C_{2h} (C_{2v}) $Cr(\eta^6\text{-}C_{10}H_8)_2$ is less than that of 0.94 in $Cr(\eta\text{-}C_6H_6)_2$ and suggests weaker bonding to the metal in the naphthalene derivative. The low-lying unoccupied molecular orbitals in $Cr(\eta^6\text{-}C_{10}H_8)_2$ are of naphthalene π^*-character with admixture of Cr d character. The presence of a weak (ϵ 25 M^{-1} cm^{-1}) absorption at 966 nm in the solution electronic absorption spectrum of $Cr(\eta^6\text{-}C_{10}H_8)_2$ is best attributed to the dipole-forbidden $16a_g \rightarrow 17a_g$ transition of the C_{2h} isomer or $16a_1 \rightarrow 17a_1$ of the C_{2v} isomer. This suggests that the calculated order of the two lowest lying unoccupied orbitals should be inverted.

Introduction

Bis(η^6-naphthalene)metal complexes of Ti,[2] V,[2,3] and Cr[2-4] have been prepared and exhibit high lability for the naphthalene ligand,[2,4] particularly when compared with the analogous benzene complexes. This observation parallels that made for several mono(arene) complexes.[5] Creation of a coordination position via an η^4-naphthalene intermediate involves less disruption of resonance energy than for an η^4-benzene[6] intermediate and may be the origin of enhanced reactivity. It was shown recently that the optical spectra of η^6-naphthalene (= η^6-Np) complexes differ from those of benzene derivatives.[2] Since theoretical calculations of the excited states have not been reported for $M(\eta^6\text{-}Np)_2$ complexes, the origin of this difference remains obscure. In particular, unlike $M(\eta\text{-}C_6H_6)_2$ compounds, the $M(\eta^6\text{-}Np)_2$ complexes can adopt two eclipsed geometries; eclipsing both rings yields the C_{2v} structure, as found in the solid state for $Cr(\eta^6\text{-}Np)_2$,[4b] while an antiparallel or slipped arrangement of the two Np ligands produces a C_{2h} structure. While this work was in progress, a revised Xα-SW calculation of $Cr(\eta\text{-}C_6H_6)_2$ appeared[7] along with results for the C_{2h} isomer of $Cr(\eta^6\text{-}Np)_2$; however, transition energies were not computed and the optical spectra were not assigned.

In this paper we report results of SCF-Xα-DV calculations for $Cr(\eta\text{-}C_6H_6)_2$ and for the C_{2v} and C_{2h} isomers of $Cr(\eta^6\text{-}Np)_2$. Optical transitions have been calculated by the Slater transition-state procedure[8] and compared with solution and solid-state spectra.

Experimental Section

Electronic absorption spectra were recorded on a Varian DMS 90 UV–visible spectrophotometer, and near IR measurements were performed on a Cary 17D spectrophotometer. The ^1H and ^{13}C NMR spectra were recorded on a JEOL FX90Q (90 MHz) spectrometer; ^1H and ^{13}C chemical shifts are reported relative to C_6D_6 used as solvent. All manipulations were performed under an atmosphere of ultra high purity argon by using standard Schlenk techniques.

Bis(naphthalene)chromium(0). This complex was prepared according to the method of Kündig and Timms.[4a] Chromium (0.4 g, 7.7 mmol) was evaporated from an alumina crucible over a period of 1 h into a cooled (−120 °C) solution of naphthalene (4 g, 31.2 mmol) in dry THF (200 mL). The pressure was maintained below 10^{-3} torr during the reaction. After filtration and removal of the solvent, unreacted naphthalene was removed by sublimation. The dark reddish black residue was recrystallized from methylcyclohexane (MCH) at −78 °C. NMR (C_6D_6): ^1H δ 4.35, 5.25, 6.90 (intensity ratio 1:1:2): ^{13}C, δ 74.8, 77.6, 123.0, 133.9, in agreement with literature values[4a] UV–visible–near-IR (THF): λ_{max}, nm (ϵ, L mol^{-1} cm^{-1}) 352 (12 000), 406 (7000), 490 (2200) 966 (25). UV–visible–near-IR (methylcyclohexane): λ_{max}, nm (ϵ, L mol^{-1} cm^{-1}) 351 (11 000), 405 (6000), 475 (1800), 955.

Bis(1-eicosylnaphthalene)chromium(0). Chromium (0.42 g, 8 mmol) was evaporated into 35 mL (90 mmol) of 1-eicosylnaphthalene (Edwards High Vacuum, "L9") at 0 °C and < 10^{-3} torr. The resulting viscous, deep red fluid was filtered through a glass frit under vacuum. Owing to the similar solubilities of complex and ligand, and to the low vapor pressure of the latter, excess ligand could not be separated from the complex. UV–visible–near-IR (MCH) λ_{max}, nm (ϵ, L mol^{-1} cm^{-1}) 357 (8500), 405 (6500), 478 (3300), 790 (90), 975 (50). UV–visible–near-IR (THF): λ_{max}, nm (ϵ, L mol^{-1} cm^{-1}) 357 (8500), 406 (6000), 478 (2600), 800 (75). The concentration of bis(1-eicosylnaphthalene)chromium in the sample was determined by measuring the amount of ligand released on decomposition in air, on the basis of the following spectral data for 1-eicosylnaphthalene. UV (MCH/THF): λ_{max}, nm (ϵ, L mol^{-1} cm^{-1}) 318 (220/260), 284 (4650/4000), 274 (4900/4200).

Calculations. Bond lengths for electronic structure calculations of $Cr(\eta^6\text{-}Np)_2$ were derived from the crystal structure[4b] and

(1) (a) University of California at San Diego. (b) University of Southern California.
(2) Morand, P. D.; Francis, C. G. *Inorg. Chem.* **1985**, *24*, 56.
(3) Henrici-Olivé, G.; Olivé, S. *J. Am. Chem. Soc.* **1970**, *92*, 4831.
(4) (a) Kündig, E. P.; Timms, P. L. *J. Chem. Soc., Dalton Trans.* **1980**, 991. Desobry, V.; Kündig, E. P. *Helv. Chim. Acta* **1981**, *64*, 1288. Kündig, E. P.; Timms, P. L. *J. Chem. Soc., Chem. Commun.* **1977**, 912. (b) Elschenbroich, C.; Möckel, R.; Massa, W.; Birkhahn, M.; Zenneck, U. *Chem. Ber.* **1982**, *115*, 334. Elschenbroich, C.; Möckel, R *Angew. Chem., Int. Ed. Engl.* **1977**, *16*, 870.
(5) Eden, Y.; Fraenkel, D.; Cais, M.; Halevi, E. A. *Isr. J. Chem.* **1976/1977**, *15* 223. Cais, M.; Kaftory, M.; Kohn, D. H.; Tatarsky, D. *J. Organomet. Chem.* **1979**, *184*, 103. Landis, C. R.; Halpern, J. *Organometallics* **1983**, *2*, 840. Crabtree, R. H.; Parnell, C. P. *Organometallics* **1984**, *3*, 1727.
(6) Albright, T. A.; Hofmann, P.; Hoffmann, R.; Lillya, C. P.; Dobosh, P. A. *J. Am. Chem. Soc.* **1983**, *105*, 3396.
(7) Weber, J.; Kündig, E. P.; Goursot, A.; Pénigault, E. *Can. J. Chem.* **1985**, *63*, 1734.
(8) Slater, J. C. *The Self-Consistent Field for Molecules and Solids: Quantum Theory of Molecules and Solids*; McGraw-Hill: New York, 1984; Vol. 4. Salter, J. C. *The Calculation of Molecular Orbitals*; Wiley: New York, 1979.

0276-7333/87/2306-0094$01.50/0

Table I. Valence Orbitals of $Cr(\eta\text{-}C_6H_6)_2$

orbital	energy, eV	% contributns from atoms Cr	C	H
$3b_{2u}$	3.5890	0	69	31
$4e_{1u}$	3.3963	0	46	54
$5e_{1g}$	3.0548	3	135	-38
$5e_{1u}$	2.8407	3	47	50
$4e_{1g}$	2.4685	1	154	-55
$4a_{2u}$	0.9881	7	22	71
$5a_{1g}$	0.3591	9	28	62
$2b_{1g}$	-1.0996	0	99	1
$2b_{2u}$	-1.7713	0	99	1
$4e_{2g}$	-3.5487	42	58	0
$4e_{1g}$	-4.4297	62	36	1
$3e_{2u}$	-4.7984	0	100	0
$4a_{1g}$[a]	-6.6251	87	8	4
$3e_{2g}$	-8.0512	57	43	0
$3e_{1g}$	-10.7640	10	89	1
$3e_{1u}$	-10.8874	0	100	0
$3a_{2u}$	-11.9774	0	99	1
$2e_{2u}$	-12.5441	0	65	35
$2e_{2g}$	-12.6135	0	63	36
$3a_{1g}$	-13.1294	0	100	0
$2e_{1u}$	-14.0900	0	87	13
$2e_{1g}$	-14.4354	4	81	15
$1b_{1g}$	-14.9944	0	59	41
$1b_{2u}$	-15.0433	0	60	40
$1b_{2g}$	-15.1412	0	100	0
$1b_{1u}$	-15.1463	0	100	0
$2a_{2u}$	-16.1485	0	85	15
$2a_{1g}$	-16.3717	2	87	11
$1e_{2u}$	-18.6237	0	95	5
$1e_{2g}$	-18.7357	0	96	3
$1e_{1u}$	-22.6885	0	100	0
$1e_{1g}$	-22.8046	1	99	0
$1a_{2u}$	-25.2235	0	100	0
$1a_{1g}$	-25.6454	0	100	0

[a] Highest occupied molecular orbital.

idealized to C_{2v} and C_{2h} geometries. The structure assumed for $Cr(\eta\text{-}C_6H_6)_2$ was that used in previous theoretical studies.[7,9] The C–H distance was chosen to be 1.08 Å. Calculations employed the SCF-Xα-DV method,[10] and numerical basis orbitals were generated via exact HFS calculations on neutral atoms. Atomic orbitals through 4d, 2p, and 1s were used as bases for Cr, C, and H, respectively. Core orbitals (1s through 3p for Cr, 1s for C) were frozen and explicitly orthogonalized against valence orbitals. The 4d orbitals were included on chromium to improve the accuracy of 1-electron transition energies calculated by the Slater transition-state method.[8] The 37 atoms in $Cr(\eta^6\text{-}Np)_2$ were grouped into four potential types: chromium, 12 carbon atoms directly bonded to chromium, 8 noncomplexed carbon atoms, and 16 hydrogen atoms. Calculations were performed with a DEC VAX 11/750 computer requiring about 12 min/iteration. Important valence molecular orbital energies and charge distributions are given in Table I for $Cr(\eta\text{-}C_6H_6)_2$ and in Table II for $Cr(\eta^6\text{-}Np)_2$. Tables of all valence molecular orbitals are available as supplementary material.

Results and Discussion

As a starting point for the computations we examined $Cr(\eta\text{-}C_6H_6)_2$, which had been computed previously by SW-Xα methods.[7,9] Valence orbital orderings, summarized in Table I, compare favorably with those of previous studies. One major difference is a uniform shift of orbital energies to lower binding energies in ref 7 compared to those found here and in ref 9a. The two reported SW-Xα studies differ greatly (~1.5 eV) in absolute energies because of different Cr sphere radii assumed.

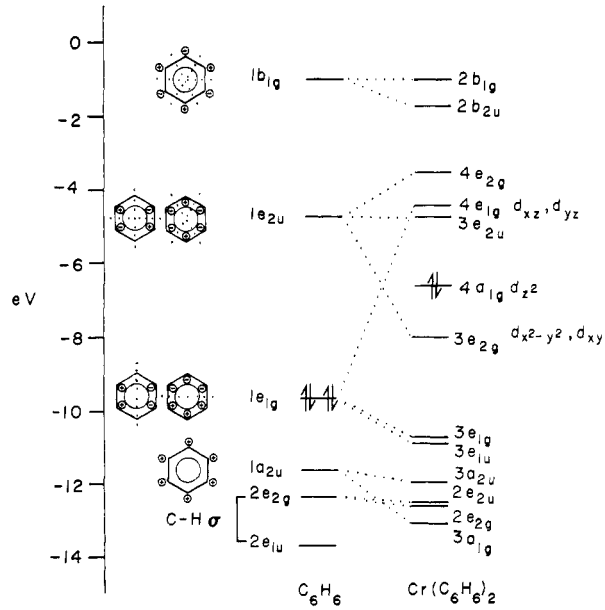

Figure 1. Results of SCF-Xα-DV calculations for C_6H_6 and $Cr(\eta\text{-}C_6H_6)_2$. The nodal pattern of the benzene π orbitals is shown and correlated with the bis(benzene)-localized π orbitals in $Cr(\eta\text{-}C_6H_6)_2$. Each benzene π orbital should be visualized as g–u pairs in making the correlation to the bis(benzene) complex.

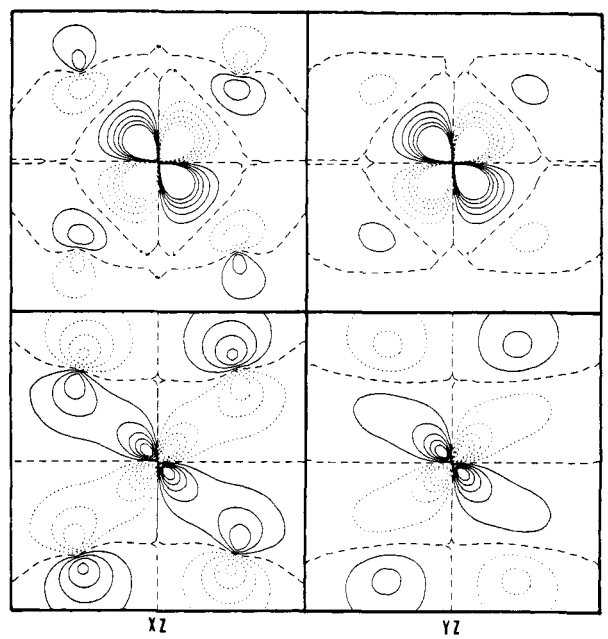

Figure 2. Orbital contour maps for the bonding $3e_{1g}$ (bottom panels) and antibonding $4e_{1g}$ orbitals (top panels) of $Cr(\eta\text{-}C_6H_6)_2$ in the xz (left) and yz (right) planes. The contour interval is 0.27 e/Å^3.

When two benzene ligands bind to chromium, the benzene π-orbitals can be divided into symmetry pairs with one being symmetric (g) and the other antisymmetric (u) with respect to the horizontal mirror plane of the complex. Correlations between the valence orbitals of benzene and those of bis(benzene)chromium are given in Figure 1. The choice of coordinates places z along the C_6 axis and x, y in the plane containing Cr and parallel to the ligand planes. Given the correlations shown in Figure 1 it appears that a ligand field model describes the fundamental interactions, with the Cr being essentially octahedral ($t_{2g} \rightleftarrows 3e_{2g}$,

(9) (a) Weber, J.; Geoffroy, M.; Goursot, A.; Pénigault, E. *J. Am. Chem. Soc.* **1978**, *100*, 3995. Note the orbital numbering scheme here differs slightly ($5e_{2g} \rightarrow 4e_{2g}$) between our work and ref. 7. (b) Ozin, G. A.; Andrews, M. P. *J. Phys. Chem.* **1986**, *90*, 1245.

(10) (a) Ellis, D. E.; Painter, G. H. *Phys. Rev. B: Solid State* **1970**, *2*, 2887. (b) Ellis, D. E.; Rosen, A.; Adadi, H.; Averill, F. W. *J. Chem. Phys.* **1979**, *65*, 3629.

Table II. Important Upper Valence Orbitals of $Cr(\eta^6\text{-}Np)_2$[a]

orbital	energy, eV	% contributns from atoms Cr	C(12)[c]	C(8)[c]
	C_{2h} Isomer			
$14b_g$	-1.1184	8	55	37
$12a_u$	-1.5746	0	50	49
$19a_g$	-1.8938	32	48	20
$16b_u$	-2.7422	1	62	38
$13b_g$	-2.7993	25	40	34
$18a_g$	-3.1651	53	40	7
$12b_g$	-3.5581	58	40	2
$11a_u$	-3.7434	0	72	28
$17a_g$	-4.7711	38	9	53
$15b_u$	-4.8352	0	50	49
$16a_g$[b]	-5.8305	84	11	2[d]
$11b_g$	-6.4576	60	19	21
$15a_g$	-7.0642	52	41	7
$10a_u$	-8.3432	0	25	75
$10b_g$	-8.8038	9	26	66
$14b_u$	-9.4050	0	45	55
$14a_g$	-9.6160	7	44	49
$9b_g$	-10.4379	10	80	9
$9a_u$	-10.5353	0	88	12
$13a_g$	-10.9296	3	46	51
$13b_u$	-11.0342	0	64	35
	C_{2v} Isomer			
$13a_2$	-1.0980	1	47	52
$13b_2$	-1.5308	8	58	34
$17b_1$	-1.9345	17	42	41
$18a_1$	-2.0582	32	56	12
$12b_2$	-2.8297	26	39	35
$12a_2$	-3.3873	36	45	19
$11a_2$	-3.6927	28	61	11
$16b_1$	-3.6971	42	56	1
$17a_1$	-4.2524	23	21	56
$15b_1$	-4.8433	13	34	53
$16a_1$[b]	-5.6847	85	11	2[d]
$11b_2$	-6.4333	58	23	19
$15a_1$	-7.0085	51	42	8
$10a_2$	-8.0842	3	17	80
$10b_2$	-8.7959	5	34	61
$14b_1$	-9.2653	6	32	62
$14a_1$	-9.5424	0	50	50
$9a_2$	-10.2952	10	83	7
$9b_2$	-10.4419	0	83	17
$13b_1$	-10.7709	4	61	34
$13a_1$	-11.1794	0	42	50[d]

[a] Lower valence orbitals are naphthalene in character with less than 10% metal contribution. [b] Highest occupied orbitals. [c] C(12) and C(8) refer to the atomic potential types composed of the twelve carbon atoms directly bonded to chromium and the eight non-bonded carbons, respectively. [d] There were small (3–8%) H-atom contributions to these orbitals.

$4a_{1g}$; $e_g \rightleftharpoons 4e_{1g}$). As expected, the empty d_{xz} and d_{yz} e_g orbitals interact with the filled benzene $1e_{1g}$ π-orbital to form the $3e_{1g}$ and $4e_{1g}$ bonding–antibonding pair. Chromium contribution to the bonding $3e_{1g}$ orbital is small (10%), and the contour maps (Figure 2) show little overlap. The highest occupied $4a_{1g}$ orbital is of Cr d_{z^2} character and nonbonding.

The unusual feature of the molecule is the covalency present in the $3e_{2g}$–$4e_{2g}$ bonding–antibonding pair, which results from the interaction between the empty benzene $1e_{2u}$ π^*-orbitals and Cr d_{xy} and $d_{z^2-y^2}$. This is effectively a δ interaction and accounts for the primary Cr–arene bonding as pointed out by Weber et al.[9a] Since the benzene $1e_{2u}$ orbital is unoccupied, the $3e_{2g}$ orbital in the complex behaves as a M → L π-bonding orbital where the electrons come from the metal. This agrees with the high charge of +0.94 calculated for the chromium center. Owing to the small metal contribution to the $3e_{1g}$ orbital, electron donation from the ligands to the metal is expected to be

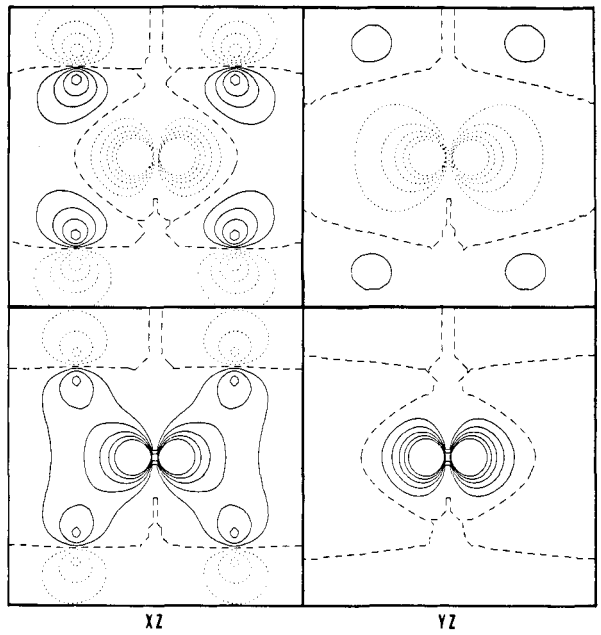

Figure 3. Orbital contour maps for the bonding $3e_{2g}$ (bottom panels) and antibonding $4e_{2g}$ (top panels) orbitals of $Cr(\eta\text{-}C_6H_6)_2$ in the xz (left) and yz (right) planes. The contour interval is 0.27 e/Å^3. The d orbital shown in $d_{x^2-y^2}$. The d_{xy} orbital also contributes to this symmetry but is not shown.

minimal. The $4e_{2g}$ orbital, which Weber et al.[9a] claim to be a π-back-bonding orbital, is seen (Figure 3) to be the M–L antibonding component of the $3e_{2g}$ orbital. Recent calculations reported[9b] for $V(\eta\text{-}C_6H_6)_2$ show a level structure similar to $Cr(\eta\text{-}C_6H_6)_2$. The use of δ symmetry metal orbitals to bind to the benzene π^*-orbitals is dictated by the δ symmetry of the benzene π^* LUMO with respect to the C_6 axis and contrasts with the situation for bis(cyclopentadienyl) complexes where the symmetry of the ligand π^*-orbital requires bonding to metal π-orbitals. Thus, the different nodal pattern of the π^*-orbitals for five- and six-membered rings accounts for the difference.

Energies and the ordering of the lowest unoccupied MO's appear to depend critically on the separations between orbitals on the benzene ligands and chromium. This becomes apparent in the SW calculations since the results change significantly with an increase in the metal sphere size.[7,9] Similar effects could be important (vide infra) in $Cr(\eta^6\text{-}Np)_2$.

The three highest occupied orbitals of the C_{2h} and C_{2v} isomers of $Cr(\eta^6\text{-}Np)_2$ (Figure 4) represent the pseudooctahedral t_{2g} metal orbitals and possess similar energies and charge distributions (Table II). The coordinate system used is defined in Figure 4. In both cases,[11] C_{2h} (C_{2v}), the HOMO is a d_{x^2} orbital of a_g (a_1) symmetry. This corresponds to the $4a_{1g}$ HOMO found for $Cr(\eta\text{-}C_6H_6)_2$. Metal–arene bonding occurs in $15a_g$ ($15a_1$), which is the interaction between the Cr $d_{y^2-z^2}$ and the bis(arene) a_{1g} orbitals, and in the low-lying $9b_g$ ($9a_2$) orbital, which combines Cr d_{xz} with the bis(arene) b_g (a_2) combination. These two bonding orbitals, along with their unoccupied antibonding counterparts, are shown in Figure 5. The $15a_g$ ($15a_1$) and $11b_g$ ($11b_2$) orbitals correspond to the $Cr(\eta\text{-}C_6H_6)_2$ bonding $3e_{2g}$ orbital. For $Cr(\eta^6\text{-}Np)_2$ the $11b_g$ ($11b_2$) molecular orbital shows no overlap between chromium and naphthalene, and for $Cr(\eta^6\text{-}Np)_2$ in C_{2h} (C_{2v}) symmetry, the $13b_g$ ($12b_2$) and $19a_g$ ($18a_1$) orbitals resemble the $4e_{2g}$ an-

(11) Completely analogous occupied orbitals exist for the C_{2h} and C_{2v} models. These orbitals will be discussed for the C_{2h} model with the equivalent C_{2v} orbitals given in parentheses.

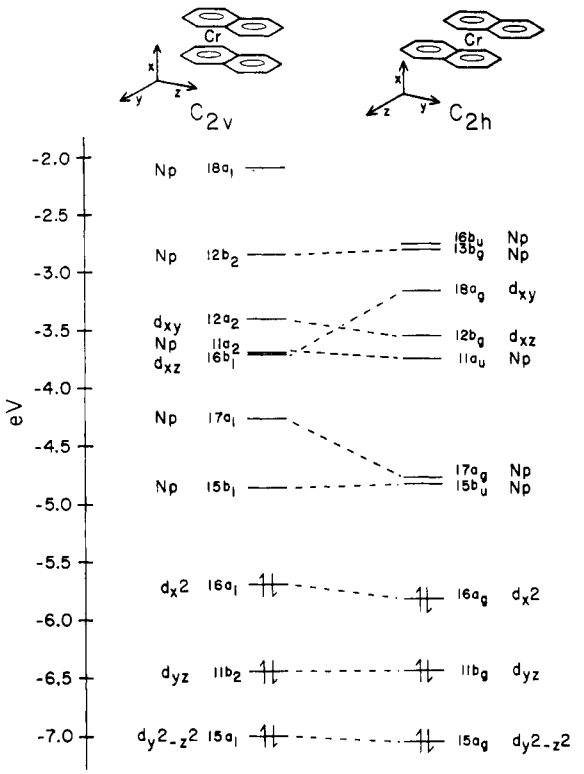

Figure 4. Molecular orbital diagram showing principal atomic character of the important valence orbitals of $Cr(\eta^6\text{-}Np)_2$ and the coordinate systems used. Note that from later analysis of experimental data we believe that the $17a_1$ and $17a_g$ orbitals should lie below $15b_1$ and $15b_u$, respectively.

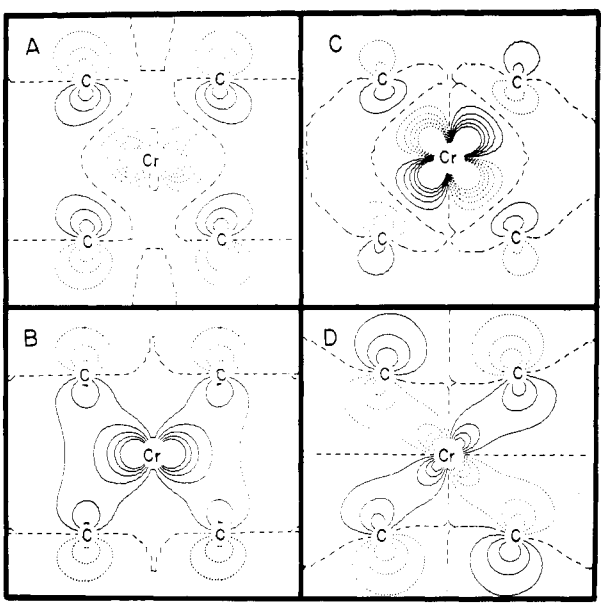

Figure 5. Principal bonding orbitals of the C_{2h} isomer of $Cr(\eta^6\text{-}Np)_2$ and their corresponding unoccupied antibonding counterparts in the xz plane: A, unoccupied antibonding $18a_g$ orbital; B, occupied $15a_g$ bonding orbital; C, unoccupied antibonding $12b_g$ orbital; D, occupied $9b_g$ bonding orbital. The contour interval is 0.04 e/Å^3. The z axis is parallel to the horizontal direction of the figure.

tibonding molecular orbital of $Cr(\eta\text{-}C_6H_6)_2$. Consistent with the occupied orbital counterparts, $13b_g$ ($12b_2$) shows little overlap between chromium and naphthalene, while $19a_g$ ($18a_1$) exhibits a strong antibonding interaction.

Examination of the total charge density contour map (Figure 6) reveals asymmetry in the xy plane for the C_{2h} model. This asymmetry results from Cr d orbitals of a_g symmetry that mix to enhance a small bonding interaction between the metal $d_{y^2-z^2}$ orbital and the out-of-phase combination of two naphthalene LUMOs (1). The $15a_g$ orbital formed is chromium–naphthalene bonding. The unoccupied antibonding counterpart, of $15a_g$ is the $18a_g$ molecular orbital that shows extensive hybridization (Figure 6A). As discussed above, the naphthalene α-carbon p_x orbitals and z-axis lobe of the chromium $d_{y^2-z^2}$ orbital form the principal Cr–Np bonding interaction (Figure 5B). In the xy plane the y-axis lobe of the $d_{y^2-z^2}$ is oriented to be weakly bonding with the β-carbon p_x orbitals (2).

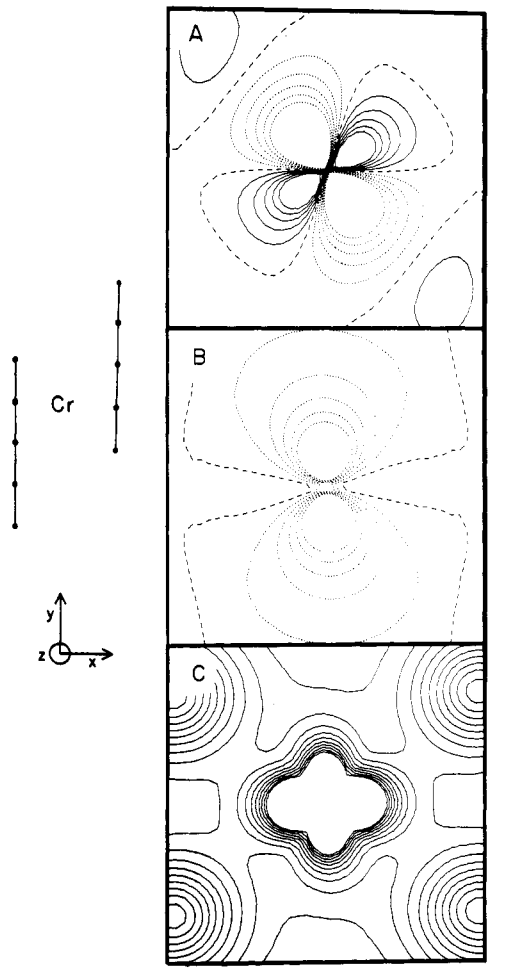

Figure 6. Orbitals of the C_{2h} isomer of $Cr(\eta^6\text{-}Np)_2$ that exhibit mixing of d_{xy} and $d_{y^2-z^2}$ shown in the xy plane: A, unoccupied $18a_g$ orbital; B, occupied $15a_g$ orbital of $d_{y^2-z^2}$ character; C, symmetric total density in xy plane. The contour interval for the wave function maps in A and B is 0.04 e/Å^3. For the total density map, C, the contour interval is 0.025 e^2/Å^3.

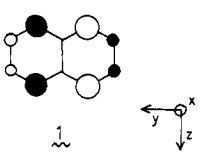

1

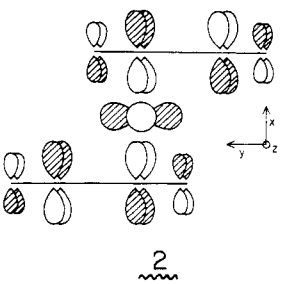

2

Table III. Population Analyses for the C_{2h} and C_{2v} Isomers of $Cr(\eta^6\text{-Np})_2$ and for $Cr(\eta\text{-}C_6H_6)_2$

$Cr(\eta^6\text{-Np})_2$, C_{2h}			$Cr(\eta^6\text{-Np})_2$, C_{2v}			$Cr(\eta\text{-}C_6H_6)_2$		
Cr	3d	4.459	Cr	3d	4.469	Cr	3d	4.304
	4s	0.089		4s	−0.027		4s	0.121
	4p	0.573		4p	0.821		4p	0.655
	4d	0.136		4d	0.029		4d	−0.018
total charge		+0.744	total charge		+0.708	total charge		+0.938
C(12)	2s	1.532	C(12)	2s	1.496	C	2s	1.551
	2p	2.598		2p	2.632		2p	2.635
total charge	per atom	−0.130	total charge	per atom	−0.128	total charge	per atom	−0.186
C(8)	2s	1.480	C(8)	2s	1.513			
	2p	2.613		2p	2.570	2.570		
total charge	per atom	−0.093	total charge	per atom	−0.083			
H(16)	1s	0.902	H(16)	1s	0.907	H	1s	0.892
total charge	per atom	+0.098	total charge	per atom	+0.093	total charge	per atom	+0.108

Hybridization of $d_{y^2-z^2}$ with d_{xy} (**3**) maximizes this bonding interaction. The y-axis lobe of the $d_{y^2-z^2}$ orbital (Figure 6B) shows distortion from the hybridization with d_{xy}, and the asymmetric total density in the xy plane (Figure 6C) is attributed to this mixing.

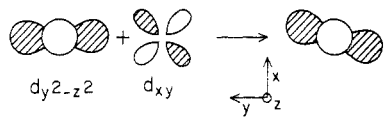

3

An analogous distortion of total charge density is possible for the C_{2v} model using Cr $d_{y^2-z^2}$ and antisymmetric naphthalene LUMOs; however, only a Cr $4p_z$ orbital has the proper symmetry to hybridize with the $d_{y^2-z^2}$ orbital (**4**). For first-row transition metals the large 3d–4p separation should result in little mixing, to yield spatially directed orbitals. Orbital and total charge density maps for the C_{2v} model support this view. That p orbitals are more important in the C_{2v} model is reflected in the Mulliken population analyses (Table III). The less favorable hybridization possible in the C_{2v} isomer may favor the C_{2h} geometry slightly over the C_{2v} structure in the gas phase or in solution even though the C_{2v} structure was found in the solid state.[4b] The major bonding contribution in both C_{2h} and C_{2v} isomers arises from preferential interactions between the metal and the peripheral carbon atoms; the two ring-fused carbon atoms lie in a nodal plane. This agrees with the solid-state structure of $Cr(\eta^6\text{-Np})_2$ that shows the metal situated slightly off the major axis.[4b]

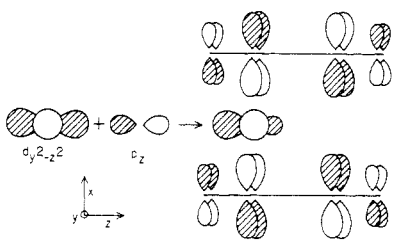

4

From the formal charge of +0.744 (0.708) for Cr in $Cr(\eta^6\text{-Np})_2$ in comparison to the value of +0.94 for Cr in $Cr(\eta\text{-}C_6H_6)_2$ (Table III) we conclude that the former compound is neutral and nonionic, in spite of the ability of naphthalene to become negatively charged. The reduced value of the metal charge in the naphthalene complexes may reflect weaker Cr → arene back-bonding. Consistent with this interpretation the Cr–ring distance is 0.05 Å longer in $Cr(\eta^6\text{-Np})_2$ than in $Cr(\eta\text{-}C_6H_6)_2$.[4b,12] Thus the enhanced lability of the η^6-Np ligand in comparison to $\eta\text{-}C_6H_6$ results not only from the preference for η^4-Np over $\eta^4\text{-}C_6H_6$ in the transition state for ring slippage,[6] but also from ground-state differences in the extent of Cr–ring bonding.

Low-lying unoccupied molecular orbitals show extensive mixing between the metal and ligand. Qualitative assignments of ligand or metal character are shown in Figure 4. Metal pseudooctahedral e_g orbitals are best represented by $12b_g$ ($16b_1$) and $18a_g$ ($12a_2$). Similar to the $Cr(\eta\text{-}C_6H_6)_2$ results, the lowest unoccupied orbitals are predicted to be ligand localized. The C_{2h} LUMO, $15b_u$, is a pure ligand orbital (required by symmetry) while the C_{2v} LUMO is primarily ligand in character with a small admixture of metal d_{xz} character. The lowest allowed electronic transition in $Cr(\eta^6\text{-Np})_2$ and $Cr(\eta^6\text{-}C_6H_6)_2$ are therefore expected to be metal-to-ligand charge transfer. The DV-Xα calculations described here conflict with experimental data for $Cr(\eta\text{-}C_6H_6)_2$ where the lowest energy transition is thought to be of metal-localized d–d character because of its low intensity.[13] This inversion in order of the first two unoccupied orbitals will be considered in the next section.

A previous SW-Xα calculation[7] for the C_{2h} isomer of $Cr(\eta^6\text{-Np})_2$ closely resembles the DV-Xα results. The HOMO–LUMO gap, however, is predicted to be ~50% greater in the Xα-SW description, and the ordering of the two lowest unoccupied orbitals is reversed in the Xα-SW model. The agreement between the orbital level schemes for the alternative computational methods is satisfactory and provides confidence in the consistency of the Xα approach.

Transition-Energy Calculations and Electronic Spectra. Calculated optical transition energies are given in Table IV. These were calculated by the Slater transition-state method[8] with a spin-restricted potential and therefore represent a mixture of singlet and triplet transition energies. Previous studies have shown[14] that singlet–singlet transitions are only about 0.1–0.2 eV to higher energy than those calculated with a spin-restricted potential. All the low-energy transitions in the C_{2h} model may be classified as metal to ligand charge transfer except for those involving the 15 and $17a_g$ orbitals, where covalency does not allow for a simple description. Qualitative assignment of all transitions in the C_{2v} model are not possible because of the high degree of covalency in the virtual orbitals.

The solution electronic absorption spectrum of $Cr(\eta^6\text{-Np})_2$ in tetrahydrofuran or methylcyclohexane (Figure 7a) consists of three intense absorptions with maxima at ~350, 405, and 480 nm, labeled I, II, and III, respectively, fol-

(12) Haaland, A. *Acta Chem. Scand.* **1965**, *19*, 41.

(13) Feltham, R. D. *J. Inorg. Nucl. Chem.* **1961**, *16*, 197.
(14) Weber, J. *Chem. Phys. Lett.* **1977**, *45*, 261.

Table IV. Comparison of Calculated and Experimental Electronic Transition Energies (eV) for $Cr(\eta^6\text{-Np})_2$

C_{2h} isomer			C_{2v} isomer	
transition	calcd energy	exptl energy[a]	calcd energy	transition
			1.20	$16a_1 \rightarrow 15b_1$
$16a_g \rightarrow 17a_g$[b]	1.56	1.29 (1.30)	1.89	$16a_1 \rightarrow 17a_1$
$16a_g \rightarrow 15b_u$	1.50		2.07	$16a_1 \rightarrow 16b_1$
$11b_g \rightarrow 15b_u$	1.81		2.31	$15a_1 \rightarrow 15b_1$
$15a_g \rightarrow 15b_u$	2.41		2.34	$11b_2 \rightarrow 17a_1$
$16a_g \rightarrow 11a_u$	2.56	2.54 (2.62)	2.70[e]	$11b_2 \rightarrow 11a_2$
			3.00	$15a_1 \rightarrow 17a_1$
$11b_g \rightarrow 11a_u$	2.90[c]	3.07 (3.07)	3.09[e]	$11b_2 \rightarrow 12a_2$
			3.09	$16a_1 \rightarrow 12b_2$
$15a_g \rightarrow 11a_u$	3.49[d]		3.29[f]	$15a_1 \rightarrow 16b_1$
$16a_g \rightarrow 16b_u$	3.59	3.54 (3.54)	3.68[e]	$11b_2 \rightarrow 12b_2$
$11b_g \rightarrow 16b_u$	3.90[c]		3.88[g]	$16a_1 \rightarrow 18a_1$
			4.18[g]	$16a_1 \rightarrow 17b_1$
$15a_g \rightarrow 16b_u$	4.50[d]		4.29[f]	$15a_1 \rightarrow 12b_2$
$16a_g \rightarrow 12a_u$	4.80		4.39[e]	$11b_2 \rightarrow 18a_1$
$11b_g \rightarrow 12a_u$	5.08[c]		5.02[f]	$15a_1 \rightarrow 18a_1$
$15a_g \rightarrow 12a_u$	5.68[d]		5.24[f]	$15a_1 \rightarrow 17b_1$

[a] Data from solution spectrum: THF (MCH). [b] Dipole-forbidden transition. [c] Energy estimated from $11b_g \rightarrow 15b_1$ transition-state calculation. [d] Energy estimated from $15a_g \rightarrow 15b_u$ transition-state calculation. [e] Energy estimated from $11b_2 \rightarrow 17a_1$ transition-state calculation. [f] Energy estimated from $16a_1 \rightarrow 12b_2$ transition-state calculation. [g] Energy estimated from $16a_1 \rightarrow 17a_1$ transition-state calculation.

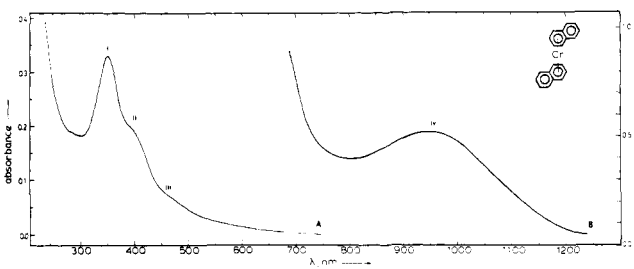

Figure 7. UV–visible (a) and near-infrared (b) spectrum of bis(η^6-naphthalene)chromium: (A) in methylcyclohexane, 2.8×10^{-4} M, 1-mm path length; (B) in tetrahydrofuran, 0.02 M, 1-cm path length.

lowed by a long tail in the visible region. The spectrum for the substituted naphthalene complex $Cr(\eta^6\text{-}C_{10}H_7R)_2$ (R = $C_{20}H_{41}$) also contains three bands that differ only in a minor fashion from Figure 7A with respect to peak position and absorptivity. Solvent has little effect on absorptivity; however, a solvent dependence was observed for the postion of band III in the spectrum of $Cr(\eta^6\text{-Np})_2$ [λ_{max} = 476 nm (MCH) and 490 nm (THF)]. While this behavior was not observed for $Cr(\eta^6\text{-}C_{10}H_7R)_2$ (R = $C_{20}H_{41}$), in other substituted-naphthalene complexes[18] this shift becomes large enough to submerge absorption III under II. Peak positions for $Cr(\eta^6\text{-Np})_2$ are compared to calculated electronic transition energies in Table IV.

The absorption of highest energy (I) correlates with three possible transitions in each symmetry. From its intensity (ϵ >10 000 L mol^{-1} cm^{-1}) it is clearly dipole-allowed, a condition that all calculated transitions in C_{2h} and C_{2v} satisfy. However, in C_{2v} $11b_2 \rightarrow 12b_2$ [which is equivalent to the $4e_{2g} \rightarrow 5e_{2g}$ excitation in $Cr(\eta^6\text{-}C_6H_6)_2$] and $15a_1 \rightarrow 16b_1$ both contain appreciable d–d character (Table II), which will decrease the LaPorte allowedness of the transitions. Band II can be equated with the transition $11b_g \rightarrow 11a_u$ in C_{2h} symmetry and $15a_1 \rightarrow 17a_1$, $11b_2 \rightarrow 12a_2$, or $16a_1 \rightarrow 12b_2$ in C_{2v} symmetry. From Table II it is seen once again that the transition in C_{2h} exhibits pure metal-to-ligand charge transfer while those in C_{2v} contain varying amounts of d–d character. A similar observation can be made for the assignment of band III (Tables II and IV).

Comparison of the observed spectrum for $Cr(\eta^6\text{-Np})_2$, in the range 300–700 nm, with the calculated transition energies (Table IV) shows good agreement, but either C_{2v} or C_{2h} symmetry provide a reasonable description of the electronic structure in solution. There may be a slight preference for C_{2v} based on the variation of the absorptivities, but it is uncertain. Since rotation of the arene rings occurs rapidly in $Cr(\eta^6\text{-}C_6H_6)_2$,[17] we expect a low barrier to rotation in $Cr(\eta^6\text{-Np})_2$. That the solution spectroscopy reflects both C_{2v} and C_{2h} symmetries is expected given the similarities between the molecular orbital orderings for the two geometries.

Calculations for both isomers (Table IV) predict a near-infrared absorption corresponding to the dipole-allowed HOMO–LUMO $16a_g \rightarrow 15b_u$ ($16a_1 \rightarrow 15b_1$) transition. In the C_{2h} case the HOMO–LUMO transition is calculated to occur at ~850 nm, while an absorption at ~1050 nm is predicted for the C_{2v} configuration. The $16a_g \rightarrow 17a_g$ ($16a_1 \rightarrow 17a_1$) transition, which is dipole and LaPorte forbidden in C_{2h} symmetry, but expected to be weakly allowed in C_{2v}, should also occur in this region. Note that the naphthalene contribution to the $17a_g$ ($17a_1$) orbital comes primarily from the uncomplexed ring of naphthalene. This should result in a poor dipole matrix element for the transition.

The solution near-infrared spectrum for $Cr(\eta^6\text{-Np})_2$, shown in Figure 7B, consists of a broad ($\Delta\lambda_{1/2}$ ~200 nm), weak absorption at 966 nm (THF)/955 nm (MCH), labeled IV. On exposure to air, band IV disappears [as do bands I–III on similar treatment of more dilute solutions] suggesting that band IV is associated with $Cr(\eta^6\text{-Np})_2$. In the solid state (KBr pellet) a similar broad band was observed with a maximum around 950–1000 nm.[15] Concentrated solutions of $Cr(\eta^6\text{-Np})_2$ absorb strongly below 700 nm, but no well-defined absorptions could be discerned in the range 500–700 nm. However, the spectrum of $Cr(\eta^6\text{-}C_{10}H_7R)_2$ contains a band at ~790 nm in addition to the absorption at 975 nm.

Because of the observation that $Cr(\eta^6\text{-Np})_2$ adopts the completely eclipsed C_{2v} structure in the solid state,[4b] it appears that the band at 950–1000 nm should be associated with the C_{2v} structure and assigned to the $16a_1 \rightarrow 15b_1$ transition (Table IV). In solution, the existence of both species, suggested by bands I–III, is not verified completely by the near IR spectroscopy since no absorption attributable to the $16a_g \rightarrow 15b_u$ (C_{2h}) transition was observed for $Cr(\eta^6\text{-Np})_2$. On placing a long alkyl chain on the naphthalene, a substitution that might be expected to favor the C_{2h} structure, an additional absorption was observed at ~790 nm, which may be the $16a_g \rightarrow 15b_u$ transition for the C_{2h} configuration.

While the energy of band IV agrees well with the calculated $16a_1 \rightarrow 15b_1$ transition energy (Table IV), its low intensity does not agree with the calculation. Similar arguments apply for the 790-nm band with respect to the $16a_g \rightarrow 15b_u$ transition. Both models predict the lowest energy transition to be an allowed MLCT transition (with some admixture of d–d character in C_{2v}), and consequently an intense absorption would be expected. The observed intensities (ϵ < 100 L mol^{-1} cm^{-1}) appear more consistent with forbidden transitions.

We mentioned previously that the DV-Xα (Table I) and SW-Xα[7] calculations for $Cr(\eta\text{-}C_6H_6)_2$ place an MLCT

(15) Because of the high concentrations of complex needed for near IR measurements, the quality of our spectra was considerably reduced by scattering.

transition below the lowest d–d transition. However, the experimental spectrum[13] suggests that the d–d transition lies at lowest energy. For $Cr(\eta\text{-}C_6H_6)_2$ a weaker Cr–benzene interaction would decrease the splitting between $3e_{1g}$ and $4e_{1g}$, dropping the $4e_{1g}$ orbital below the $3e_{2u}$ benzene π^*-combination orbital. The $4a_{1g}$ to $3e_{2g}$ splitting would also decrease (effectively this is decreasing $10Dq$). Although the orbital combinations are not identical in naphthalene and benzene, the existence of a similar effect could place the $17a_g$ ($17a_1$) orbital below $15b_u$ ($15b_1$) in $Cr(\eta^6\text{-Np})_2$ (Figure 4). If the $15b_u$ and $15b_1$ orbitals lie at higher energy, near $11a_u$ and $16b_1$, the spectral correlation is more consistent. Given the inaccuracies in existing MO models for metal complexes, a result of the frozen core approximation and potential and exchange energy approximations as well as the crude description of excited state virtual orbitals by minimal basis set calculations, such an error could well occur. The most satisfactory assignment for the weak intensity of absorption IV (Figure 7B) therefore appears to be $16a_g \rightarrow 17a_g$ ($16a_1 \rightarrow 17a_1$), which is a dipole-forbidden transition in C_{2h} and expected to be weakly allowed in C_{2v}. The presence of the additional absorption at 790 nm for $Cr(\eta^6\text{-}C_{10}H_7R)_2$ suggests it be assigned to the C_{2h} isomer and band IV to the C_{2v} isomer.

Conclusions

Major differences between the spectra of $Cr(\eta^6\text{-}C_{10}H_2)_2$ and bis(benzene)chromium can be interpreted in terms of a lower symmetry in the former complex. The observation that the UV–visible spectra are not described uniquely by a C_{2v} or C_{2h} geometry can be rationalized if the complex possesses a low barrier to rotation for the arene rings. This suggests that a probe of the ring rotation in these bis(naphthalene) complexes is necessary. On substituting the naphthalene ring with an alkyl group, only minor changes are observed in the electronic spectra, the most noteworthy being the appearance of a weak absorption at 790 nm. This suggests that the electronic structure is relatively insensitive to the substituents on the ring and to which ring is complexed.

Finally, some low-energy unoccupied orbitals in $Cr(\eta^6\text{-}C_{10}H_2)_2$ are predicted to contain dominant naphthalene π^*-character. We reported recently[16] the observation of an apparently stable bis(naphthalene)iron complex, which represents an unusual 20-electron configuration. That the two electrons added, on progressing from Cr to Fe, could be delocalized on the arene ring may account for this stability.

Acknowledgment. This material is based on work supported by the National Science Foundation (CHE-8504088 to W.C.T. and CHE-8506032 to C.G.F.). W.C.T. thanks the Sloan Foundation for a research fellowship. We thank Dr. A. E. Stiegman and M. Heinrichs (California Institute of Technology) for help in obtaining the near IR spectra, Dr. D. Liston (USC) for sharing his glovebox, and P. R. Morton for recording NMR spectra.

Registry No. $Cr(\eta^6\text{-}C_6H_6)_2$, 1271-54-1; $Cr(\eta^6\text{-}C_{10}H_8)_2$, 33085-81-3; Cr, 7440-47-3; bis(1-eicosylnaphthalene)chromium(0), 105205-39-8; 1-eicosylnaphthalene, 93646-23-2.

Supplementary Material Available: Complete tables of orbital energies and atomic character for the C_{2v} and C_{2h} isomers of $Cr(\eta^6\text{-Np})_2$ (4 pages). Ordering information is given on any current masthead page.

(16) Morand, P. D.; Francis, C. G. *Organometallics* **1985**, *4*, 1653.
(17) Rotation around the arene–M–arene axis for various $M(\eta\text{-}C_6H_6)_2$ species in solution at room temperature has been postulated on the basis of NMR, ESR, and ENDOR measurements. See, for example: Campbell, A. J.; Fyfe, C. A.; Harold-Smith, D.; Jeffrey, K. R. *Mol. Cryst. Liq. Cryst.* **1976**, *36*, 1. Mulay, L. N.; Rochow, R. G.; Fischer, E. O. *J. Inorg. Nucl. Chem.* **1957**, *4*, 231. Prins, R.; Reinders, F. J. *Chem. Phys. Lett.* **1969**, *3*, 45. Schweiger, A.; Wolf, R.; Günthard, H. H.; Ammeter, J. H.; Deiss, E. *Chem. Phys. Lett.* **1980**, *71*, 117.
(18) Spare, N. J. Ph.D. Thesis, University of Southern California, 1985.